NOTICE

CERTAIN DATA CONTAINED IN THIS DOCUMENT MAY BE DIFFICULT TO READ IN MICROFICHE PRODUCTS.

CONF-9009173--1

1394 12

Note: This is a preprint of a paper being submitted for publication. Contents of this paper should not be quoted nor referred to without permission of the author(s).

CONF-9009173--1

DE91 000721

[Invited Paper: Conference on *Progress in High-Temperature Superconducting Transistors*, The International Society for Optical Engineering (SPIE), (Oct. 4–5, 1990, Santa Clara, CA), SPIE Proceedings Vol. 1394]

Growth and transport properties of Y-Ba-Cu-O/Pr-Ba-Cu-O superlattices

Douglas H. Lowndes, David P. Norton, J. D. Budai, D. K. Christen, C. E. Klabunde, R. J. Warmack,* and S. J. Pennycook

Solid State Division
*Health and Safety Research Division
Oak Ridge National Laboratory
P. O. Box 2008
Oak Ridge, Tennessee 37831-6056
operated by
MARTIN MARIETTA ENERGY SYSTEMS, INC.
for the
U.S. DEPARTMENT OF ENERGY
under contract DE-AC05-84OR21400

Growth and transport properties of Y-Ba-Cu-O/Pr-Ba-Cu-O superlattices

Douglas H. Lowndes, David P. Norton, J. D. Budai, D. K. Christen,
C. E. Klabunde, R. J. Warmack,* and S. J. Pennycook

Oak Ridge National Laboratory
Solid State Division
*Health and Safety Research Division
P.O. Box 2008, Oak Ridge, TN 37831-6056

ABSTRACT

The pulsed-laser deposition method has been used to fabricate epitaxial, nonsymmetric M(Y) × N(Pr) superlattices in which $YBa_2Cu_3O_{7-x}$ (YBCO) layers either M = 1, 2, 3, 4, 8, or 16 c-axis unit cells thick are separated by insulating $PrBa_2Cu_3O_{7-x}$ (PBCO) layers N unit cells thick (N = 1 to ~32). The zero-resistance superconducting transition temperature, T_{c0}, initially decreases rapidly with increasing PBCO layer thickness, but then saturates at T_{c0} ~ 19 K, 54 K, 71 K, or 80 K, for structures containing 1-, 2-, 3-, or 4-cell-thick YBCO layers, respectively. Critical current density measurements carried out on structures with 16- or 32-cell thick YBCO layers show that the magnitude of $J_c(H = 0) \sim 1\text{-}2\ MA/cm^2$, as well as the magnetic field dependence and the anisotropy of $J_c(H)$ all are in good agreement with corresponding measurements on thicker, single-layer YBCO films. Thus, there is no evidence of an enhanced $J_c(H)$ due to the multi-layered structure, for the layer thicknesses investigated to date. The systematic variation of T_{c0}, as a function of the YBCO and PBCO layer thicknesses, is discussed in light of other recent experiments and theoretical model calculations. The superlattices' structural and compositional order are characterized using x-ray diffraction, transmission electron microscopy, and scanning tunneling microscopy, and details of the pulsed-laser deposition process are reported.

1. INTRODUCTION

The use of high-temperature superconductors (HTSC) in active devices, and especially in hybrid superconductor/semiconductor electronics, is expected to require multilayered structures in which epitaxial insulator and/or metal layers are grown on a single-crystal substrate in combination with epitaxial HTSC layers that have excellent superconducting properties. For some applications (e.g., tunneling) abrupt, high-quality interfaces are required, and this has resulted in considerable recent interest in in situ film-growth techniques by which epitaxial layers can be grown sequentially without breaking vacuum. Recent research has established that there are a number of substrate/epitaxial buffer (or tunneling) layer combinations that are compatible, in varying degrees, with subsequent in situ epitaxial growth of $YBa_2Cu_3O_{7-x}$ (YBCO) films or multilayered M-123 structures (M = Y or a rare earth). The epitaxial buffer layer/substrate combinations demonstrated to date include Y_2O_3 and $SrTiO_3$ (both on MgO)[1,2]; $MgAl_2O_4$,[3] $BaTiO_3/MgAl_2O_4$,[4] CaF_2,[5] yttria-stabilized cubic ZrO_2(YSZ),[6,7] Al_2O_3,[8] and PrO_2 (all on silicon)[9]; and MgO,[10,11] ZrO_2,[12] YSZ [12] and $SrTiO_3$ (all on sapphire, Al_2O_3).[13] One difficulty encountered in sequentially growing epitaxial YBCO layers on top of these structures is that the optimum ambient oxygen pressure and substrate temperature in general will differ, requiring either that compromises are made or that the ambient conditions are changed with attendant delays between layers. Other compromises also may be required, for example between the amount of ambient oxygen needed to grow the highest quality insulating layers and the need to reduce oxygen pressure to avoid rapid oxidation of the substrate itself (e.g., using silicon).[7]

Our own work has focused recently on using the pulsed-laser ablation method to grow and study the superconducting properties of epitaxial $YBa_2Cu_3O_{7-x}/PrBa_2Cu_3O_{7-x}$ (YBCO/PBCO) superlattices that contain up to 80 layers (40 periods of compositional modulation).[14, 15] The superconducting YBCO layers can be as thin as a single unit cell in these structures. PBCO is interesting and useful because it is a semiconductor at room temperature with an a-b plane lattice mismatch of only ~1.5% with YBCO, and it is the only non-metallic member of the M-123 family that easily grows as single-phase material.[16,17] A final, important advantage of PBCO for superlattice growth and subsequent studies is that oxygen diffuses readily through it, so that fully oxidized YBCO/PBCO superlattices can be formed by the same in situ process that is used for entirely superconducting YBCO films. The YBCO/PBCO system also has been investigated extensively by groups at Geneva,[19,20] Rutgers,[21] and Bellcore,[22–25] including growth of epitaxial $Y_{1-y}Pr_yBa_2Cu_3O_{7-x}$ alloy films that display a wide range of resistivities, and heterostructures incorporating them.[23–25]

In this paper we briefly review the PLA method and the conditions that we have used to obtain very smooth, c-axis-perpendicular (c-perp) YBCO and PBCO films. Then we discuss the structural characteristics of YBCO/PBCO superlattices, as determined by x-ray diffraction (XRD), scanning tunneling microscopy (STM), and transmission electron microscopy (TEM). Next, we show results of electrical transport measurements that reveal the systematic variation of T_c that is found, as a function of the superconducting and insulating layer thicknesses. We also briefly review several possible explanations for this variation. Finally, we present results that demonstrate that superlattices with YBCO layer thicknesses of ~ 20–40 nm have critical current densities that are just as high, and with similar anisotropy, as for much thicker single-layer YBCO films.

2. FILM GROWTH BY PULSED LASER ABLATION

Our superlattices were grown by mounting stoichiometric YBCO and PBCO targets in a multi-target holder that permits target rotation during ablation and target exchange. A pulsed KrF (248 nm) laser beam was brought to a horizontal line focus on the rotating target and was simultaneously repetitively scanned over the target in the vertical direction, in order to produce a region of only slowly varying film thickness on the substrate heater located ~6.5 cm. away. KrF, together with XeCl, shares several advantages for laser-ablation film growth, including high laser power, a sufficiently large absorption coefficient, and widely available coated optics (mirrors, etc.), in comparison with either longer or shorter laser wavelengths. Epitaxially polished (100) $SrTiO_3$ substrates were bonded to the stainless steel heater plate using silver paint. The ability to grow smooth films is particularly important for superlattice fabrication. Our superlattices were grown at a heater (substrate) temperature of 730°C (~670°C) because we earlier found that this temperature produces very smooth thicker YBCO films. Increasing the heater temperature by 50°C produces YBCO films that SEM inspection shows to have a slightly pitted morphology, at least in some regions of the ablation plume. Both single-layer films and superlattices were grown in 200 mTorr oxygen at a deposition rate of 1.1 Hz and ~0.1 nm/laser pulse. After deposition samples were cooled at 10°C/min in oxygen, the oxygen pressure being increased slowly to reach ~600 Torr at 600°C and then held constant. Superlattice periods that were measured directly by XRD agreed to within a few percent with those calculated from the measured superlattice thickness and number of laser shots.

In earlier work,[26] it was shown that the single-layer YBCO films grown on a variety of (100) substrates under very similar conditions were very smooth, specularly reflecting, and highly c-perp-oriented, with $T_c(R = 0) > 92$ K, $\Delta T_c < 1$ K, and $J_c \sim 2$ MA/cm^2 for the best films. Figure 1 is an STM micrograph of a ~30 nm wide pinhole defect in such a single-layer YBCO film, and illustrates directly YBCO's c-perp growth habit and highly layered structure when grown under these conditions. The terraces shown in Fig. 1 were measured to be ~12 Å thick, corresponding to |c| ~11.7 Å for YBCO. We note that Inam et al. recently have developed a technique for growing YBCO films that are > 95% in the a-perp orientation, using an a-perp PBCO template layer that was deposited prior to the YBCO at a lower substrate temperature.[27] Although the transport properties of their a-perp YBCO films are inferior to c-perp YBCO (apparently because of twin boundaries between grains that correspond to the two possible c-axis orientations in the substrate plane), further development of this technique may make possible growth of a-perp superlattices in the YBCO/PBCO system.

Figure 1. Scanning tunneling micrograph of a surface defect in a laser-ablated YBCO film, illustrating its highly c-perp-oriented growth mode. The area shown is 40 nm on each side; most of the vertical steps are 1.2 nm (~|c|) high.

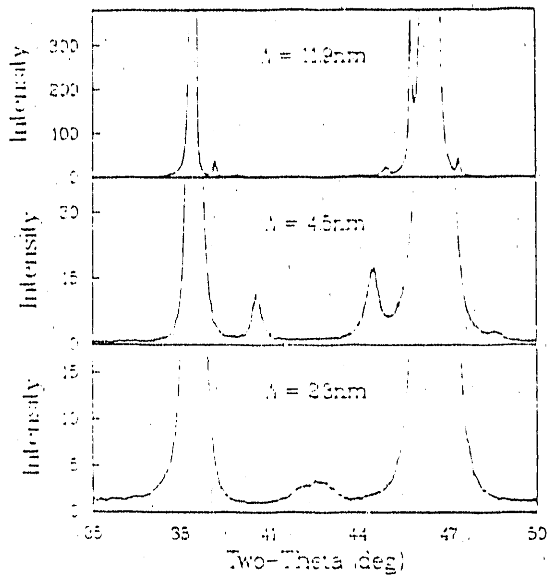

Figure 2. θ–2θ x-ray diffraction scans along the (00ℓ) axis from nominally M = 1 YBCO/PBCO superlattices with modulation wavelengths of Λ = 2.3 nm (30 periods), Λ = 4.5 nm (30 periods), and Λ = 11.9 nm (20 periods). Note the higher-harmonic sidebands for the latter structure.

3. EPITAXIAL YBCO / PBCO SUPERLATTICES

3.1 Structural characterization

We have fabricated epitaxial, nonsymmetric MxN superlattices in which YBCO layers M unit cells in thickness (with M ranging from 1 to ~32) are separated by insulating PBCO layers N unit cells thick (with N ranging from 1 to ~16).[14, 15] Figure 2 shows XRD spectra for three different YBCO/PBCO superlattices in which the YBCO layers are approximately one unit cell thick. The two large peaks (truncated) in each scan correspond to the superlattice (005) and the $SrTiO_3$ (002) + superlattice (006) peaks. XRD θ–2θ scans revealed only (00ℓ) diffraction peaks, indicating that the only crystalline phase present has its c-axis aligned with the (00ℓ) of the $SrTiO_3$ substrate. Rocking curves (θ-scans) through the (00ℓ) peaks showed that the mosaic spread of the atomic planes lying parallel to the substrate surface is excellent, typically less than 0.4° full width at half maximum (FWHM). In addition, the position and width of (hkℓ) Bragg peaks with h, k≠0 were measured and revealed that the in-plane epitaxy is such that the <110> directions of the film and the substrate are aligned (in-plane mosaic spread ≤0.5°), as has been observed previously for pure YBCO films on perovskite substrates.[25]

The "signature" of a periodic superlattice is that each (00ℓ) peak in Fig. 1 is modulated by diffraction sidebands (satellite peaks). The modulation wavelength (the sum of consecutive layer thicknesses) can be calculated from the satellite positions using the equation[29] $\Lambda = \lambda/2(\sin\theta_i - \sin\theta_{i-1})$, where here λ = 0.15406 nm is the $CuK\alpha_1$ x-ray wavelength and θ_i and θ_{i-1} are the Bragg angles for consecutive diffraction maxima. The modulation wavelengths derived from the top and bottom panels in Fig. 2 show that these superlattices have compositions very close to 1×9 and 1×1, respectively. The middle panel shows the XRD from an "imperfect"

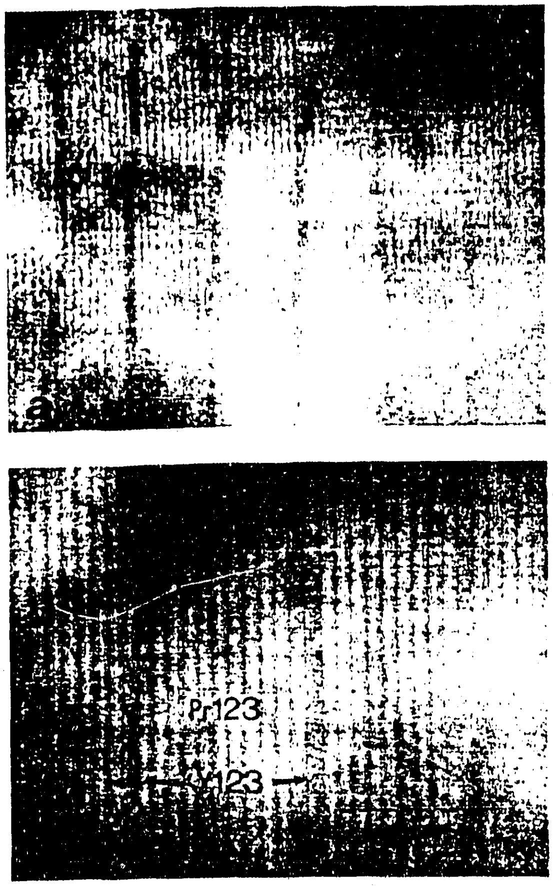

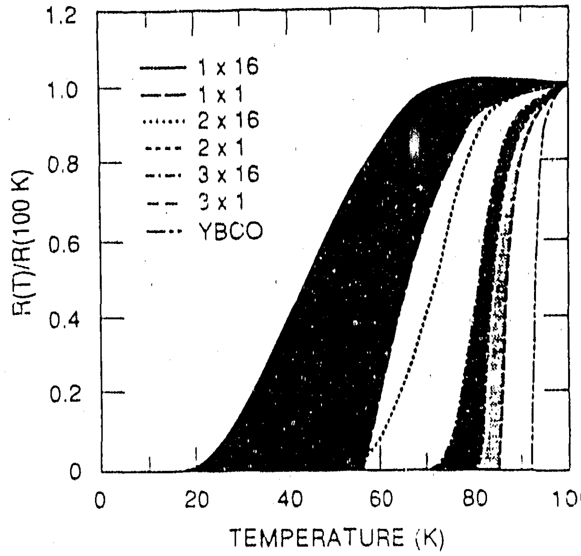

Figure 4. Normalized resistance, R(T)/R(100 K), vs. temperature for nonsymmetric M(YBCO) × N(PBCO) superlattices containing M = 1-, 2-, or 3-cell-thick YBCO layers and either 1- or 16-cell-thick PBCO layers. The superconducting transition for a pure YBCO film also is shown.

Figure 3. High-resolution cross-section Z-contrast TEM image of a compositionally imperfect YBCO/PBCO superlattice. The bright regions are PBCO, dark are YBCO. The vertical lines correspond to successive c-axis unit cells ($|c| \sim 1.17$ nm).

superlattice, for which the modulation wavelength corresponds compositionally to a "3/4 × 3" structure, i.e., the switching between YBCO and PBCO targets resulted in only about 3/4 of a unit cell being filled with YBCO, on average, at the location on the substrate heater where this structure was grown. Consequently, this "alloy superlattice" had a T_c that was depressed below the results that are given below for 1×N structures. However, the most significant feature of Fig. 2 is the presence of observable satellite intensity, and hence direct evidence of a Y/Pr compositional modulation, for all of the 1×N structures. For the $\Lambda = 2.3$ nm (1×1) structure, which was deposited as alternating single-unit-cell thick layers of YBCO and PBCO, the clear implication is that interdiffusion must be limited to less than a single unit cell during the in situ laser ablation growth process. The fact that XRD shows chemical modulation to be present even for an imperfect superlattice (Fig. 2, middle) confirms that interdiffusion and cation mobility must be very small along the growth (c-axis) direction, consistent with high lateral cation mobility, the c-perp growth mode, and the layered structure of these materials.

Figure 3 shows what we believe to be the first Z-contrast cross-section TEM image of a YBCO/PBCO superlattice. The Z-contrast method[30,31] uses Rutherford-scattered electrons for image formation and so provides chemical sensitivity directly. The particular sample shown in Fig. 3 was grown in an uncalibrated region of the laser ablation beam, so that YBCO/PBCO target switching resulted in a structure that was chemically ~1.25(Y) + 10(Pr) on average, rather than 1×8. Nevertheless, the ~ single-cell-thick dark (YBCO) layers alternating with ~8-11 bright (PBCO) layers shown in Fig. 3 provides direct confirmation that our 1×N superlattices do contain single-cell-thick YBCO layers with sharp interfaces, well-defined compositional modulation, and minimal interdiffusion. We note, though, that the dark YBCO regions shown in Fig. 3 occasionally "jump" from one structural cell to another, rather than alloying equally into two adjacent cells. We originally thought that this might indicate a tendency toward phase separation[17] of YBCO in PBCO, which would provide a mechanism for stabilizing YBCO/PBCO superlattices against interdiffusion along the c-axis. To test this idea, we recently grew $Y_{0.3}Pr_{0.7}Ba_2Cu_3O_{7-x}$ alloy thin films, which are not superconducting, and subjected them to a series of long-term, low-oxygen-pressure anneals, to see if any tendency toward superconductivity would develop as a result of YBCO phase separation. No such effect was seen. Thus, we have no direct evidence of a phase-separation mechanism for stabilization of YBCO/PBCO superlattices, and the "jumping" seen in Fig. 3 may simply be an artifact connected with the "overfilling" of the YBCO layers in this particular specimen. Further Z-contrast studies are planned in order to investigate this question.

Information concerning the extent of both structural and compositional order can be obtained from the x-ray peak widths since these widths are inversely related to the average domain size via the Scherrer equations.[32] We find that the widths of the main (00ℓ) peaks increase only slightly with order and yield domain sizes on the order of the film thickness. Since these widths are related to the overall crystalline coherence of the M-123 phase,[19] we conclude that the films are extremely well ordered structurally. In contrast, we find that the widths of the superlattice reflections increase more rapidly with order and yield coherence lengths several times smaller than the film thickness. Since these widths are related to the coherence of the Y/Pr composition modulation, we conclude that although the superlattices are fairly well ordered, the periodicity of the chemical order is not perfectly constant throughout the film, consistent with Fig. 3.

3.2 Electrical Transport Properties

Figure 4 shows the normalized resistances, R(T)/R(100 K), for YBCO/PBCO superlattices with 1-, 2-, and 3-cell thick YBCO (superconducting) layers and either 1- or 16-cell thick PBCO (insulating) layers. Similar data were obtained for intermediate PBCO layer thicknesses,[14] and resulted in normalized resistance curves that lie between those shown, but those data are not shown for clarity. The peak in the normalized resistance for the 1×16 structure is a consequence of conduction through a structure that consists of insulating (PBCO) and metallic (YBCO) layers that are electrically in parallel. The temperature at which the peak occurs depends on the relative thicknesses of the two types of layers, and similar peaks are found for the other structures above 100 K.

The most striking feature of Fig. 4 is that for the of 1-, 2-, or 3-cell-thick YBCO layers, the normalized resistance and the zero-resistance transition temperature, T_{c0}, vary systematically, and the normalized resistance for an arbitrary PBCO thickness lies within the appropriate 1-, 2-, or 3-YBCO-cell "manifold" of resistive behavior (shown shaded in Fig. 4). The manifolds of 1×N and 2×N behavior do not overlap appreciably below 100 K, and the 2×N and 3×N manifolds only partially overlap. For a fixed YBCO layer thickness, T_{c0} decreases as the thickness of the insulating PBCO layers increases. However, in going from 1-cell to 2-cell-thick YBCO layers, the spread in T_{c0} values corresponding to the full range of PBCO thicknesses decreases dramatically, and in going from 2-cell to 3-cell-thick YBCO layers the spread in T_{c0} values decreases again. From these observations it also can be seen that although the 1×1, 1×2, and 1×4 structures have the same average composition as the 2×2, 2×4, and 2×8 structures, respectively, they have very different T_{c0} values. These striking differences in resistive behavior, for structures that have the same average composition, together with the sharp satellite peaks shown in Fig. 2, demonstrate that we are observing the superconducting behavior of periodically layered superconducting structures and not of average alloys.

Figure 5 shows that for all of the M×N superlattices (with M = 1, 2, 3, 4, and 8), increasing the thickness of the PBCO layers results in an initial decrease of T_{c0}, followed by saturation of T_{c0} at a nonzero value for large PBCO layer thicknesses. Thus, even the Cu-O bilayers in a single-cell-thick YBCO layer are

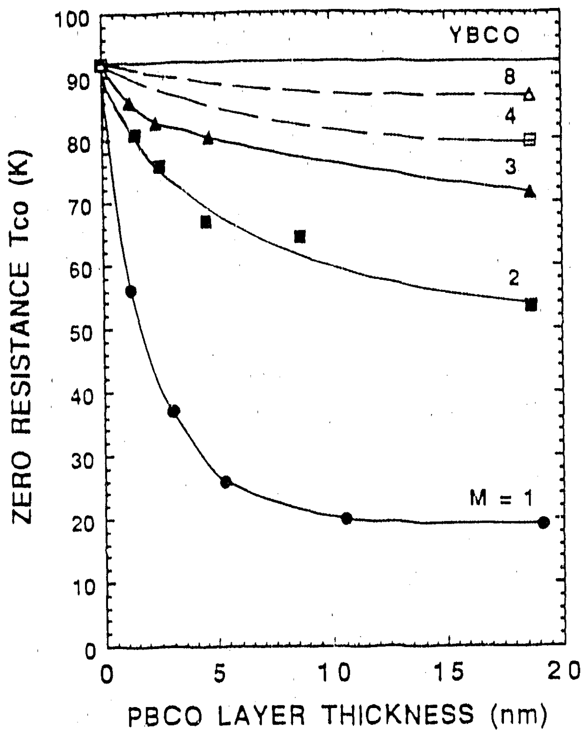

Figure 5. Zero-resistance superconducting transition temperature, T_{c0}(K), vs. PBCO layer thickness for nonsymmetric YBCO/PBCO superlattices containing 1- (●), 2- (■), 3- (▲), 4- (□), and 8- (Δ) cell-thick YBCO layers and for pure YBCO (solid line).

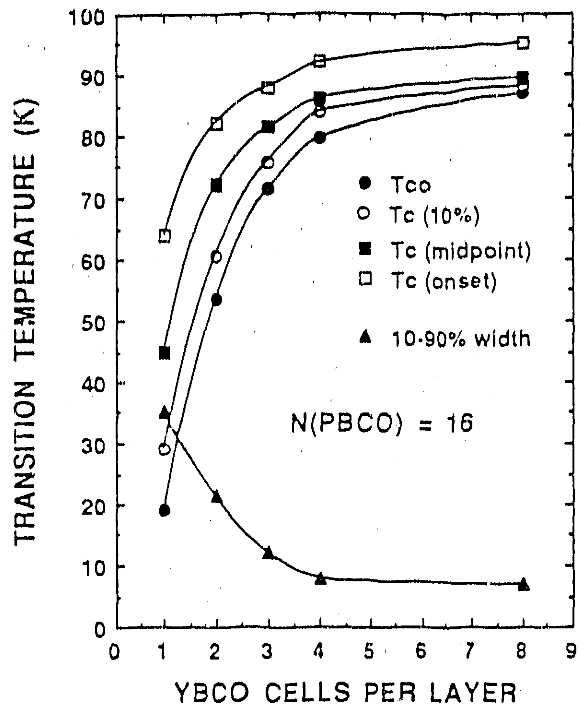

Figure 6. Superconducting transition temperatures and 10–90% transition width vs. number of YBCO cells per superconducting layer, for YBCO/PBCO superlattices in which the insulating PBCO layers are 16 unit cells thick.

superconducting with $T_{c0} \sim 19$ K, when embedded in a thick PBCO matrix. Figure 5 also shows that the T_{c0} values for M(YBCO) x N(PBCO) superlattices are very different from those of alloys having the same average composition. For large PBCO layer thicknesses, T_{c0} saturates for all of the superlattices, while T_{c0} for Pr-rich alloys goes to zero.[16,17]

Furthermore, we find that both the initial rate and the overall magnitude of the decrease in T_{c0} with increasing PBCO thickness depends sensitively on the number of adjacent YBCO cells in the superconducting YBCO layer. Figures 5 and 6 show that for well-isolated YBCO layers [i.e., N(PBCO) = 16)], only the single-cell-thick YBCO layers have very broad transitions and low T_{c0}. With increasing YBCO layer thickness, the 10–90% transition width narrows and T_{c0} rises rapidly, so that a 3-cell-thick YBCO layer has $T_{c0} \sim 71$ K, and $T_{c0} \sim 80$ K for a 4-cell-thick YBCO layer. Similarly, a 2x8 structure (only 20% YBCO on average) has a higher T_{c0} than a 1x1 structure (50% YBCO on average). These results demonstrate the importance of having YBCO in adjacent unit cells in order to raise T_{c0}, and suggest either that coupling is necessary between YBCO cells in order to <u>increase</u> their T_{c0}, or that T_{c0} is inherently high (~ 92 K) in YBCO and it is only those YBCO cells that are immediately adjacent to PBCO that have their T_{c0} depressed by proximity to PBCO. In particular, PBCO is not very effective in depressing T_{c0} if the YBCO layers are much thicker than one unit cell (see discussion below).

3.3 Critical Current Densities in YBCO/PBCO Superlattices

Christen et al.[33,34] and Roas et al.[35] have reported large anisotropies in the critical current densities, $J_c(H)$, of epitaxial YBCO films, depending upon whether the applied magnetic field, H, is aligned parallel to

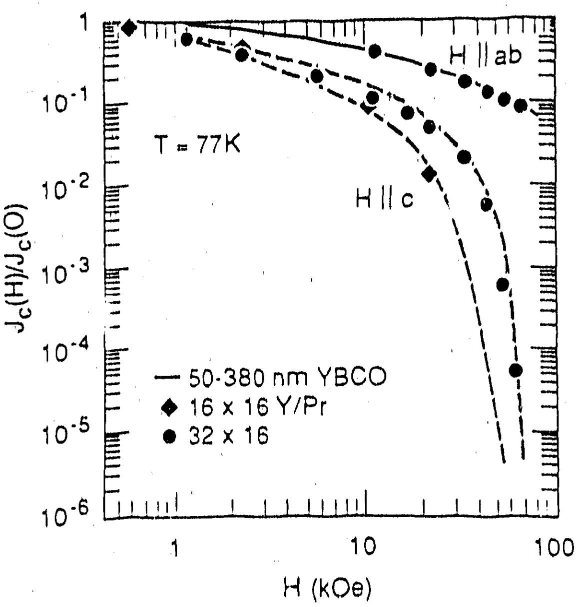

Figure 7. Normalized $J_c(H)$ at T = 77 K for single-layer epitaxial c-axis-perpendicular YBCO films with thicknesses of ~50–380 nm, for H parallel to the a-b (Cu-O) planes (solid line) or to the c-axis (dashed lines and stippled region). Also shown are data for 32×16 (circles) and 16×16 (diamonds) YBCO/PBCO superlattices.

the copper-oxygen (a-b) planes or parallel to the c-axis. As illustrated in Fig. 7, enhanced $J_c(H)$ values and a reduced dependence on H were found when H was aligned precisely parallel to the a-b planes, for single-layer YBCO films that ranged in thickness from ~ 50–380 nm. For H | | a-b at 77 K, the $J_c(H)$ data lie on a universal curve, indicating a common flux-pinning mechanism for the different specimens with $J_c(H)$ nearly independent of film thickness (i.e., a bulk flux-pinning effect is observed). The data also exhibit only a weak field dependence at 77 K, with $J_c > 10^5$ A/cm^2 at 8 T., indicating a flux-pinning energy barrier that is significantly greater than k_BT for this orientation. In contrast, for H | | c Christen et al. find that $J_c(H)$ at 77 K decreases rapidly for H fields greater than 2-4 T., and displays order-of-magnitude variations from sample to sample.[33,34] They also carried out similar experiments using YBCO films grown epitaxially on $SrTiO_3$ substrates whose surfaces were deliberately miscut at an angle of 6° to the crystal lattice (001) planes, and confirmed that the enhanced J_c for H | | a-b is associated with the layered crystal structure itself, and is not a result of "surface pinning" due to having H parallel to the film surface. The sample-dependent variations in J_c for H | | c are believed to reflect differences in the flux-pinning defect structures that were "grown-into" the films by uncontrolled differences in processing. For H | | a-b, further experiments led them to conclude that the enhanced J_c results either from "intrinsic" pinning when fluxoids are located in the nonsuperconducting regions of the layered structure, or is caused by a flux-pinning defect structure that is itself highly anisotropic.[34]

These observations of bulk but orientation-dependent flux-pinning in thicker YBCO films naturally raise questions of whether similar effects will be seen in very thin films, and whether additional flux pinning and enhancements of $J_c(H)$ might occur in superlattice structures that contain "internal surfaces" at the interfaces between superconducting (YBCO) and insulating (PBCO) layers, or in which the relaxation of strain fields above a critical layer thickness is accompanied by formation of defects such as misfit dislocations. To study these questions, we have initiated experiments using both 32×16 (5 periods) and 16×16 (5 periods) YBCO/PBCO superlattices. Superlattices containing relatively thick YBCO layers were used in order to keep $T_c(H=0)$ well above 77 K and make possible direct comparisons with the behavior of the much thicker single-layer epitaxial YBCO films at 77 K. Direct-current measurements of $J_c(H)$ were made using superlattices patterned with bridges 3 mm long × 0.1 mm wide and an electric field criterion for J_c of 1 μV/cm. As shown in Fig. 7, the normalized $J_c(H)$ behavior of these superlattices is virtually identical to that of the thicker, single-layer YBCO films, i.e. $J_c(H)$ is enhanced for H | | a-b but falls off with increasing H for H | | c. For both orientations the magnitude of the normalized $J_c(H)$ is in good agreement with the range of values typical of thicker films, i.e., these superlattices and single-layer YBCO films display the same $J_c(H)$ anisotropy. The $J_c(H = 0)$ values were ~1.5 MA/cm^2 and ~1.9 MA/cm^2 for the 32×16 and 16×16 superlattices, respectively, completely consistent with the ~ 2 MA/cm^2 value that is typical of single-layer YBCO films grown under the same conditions. Thus, there is no evidence in these initial results at T = 77 K of any enhancement of $J_c(H)$ due to the superlattice structure.

4. DISCUSSION

4.1 Variation of T_c in Superlattice Structures

The results presented in Figs. 4 and 5 show that T_{c0} is nonzero for thin YBCO layers that are isolated from each other by PBCO layers up to ~19 nm thick. In particular, the two Cu-O planes in single-cell-thick YBCO layers are superconducting with T_{c0} ~ 19 K, when embedded in a PBCO matrix. As pointed out above, the T_c values for our M×N superlattices are very different than those for alloys having the same average composition: T_{c0} saturates for large PBCO layer thicknesses, while T_c for Pr-rich alloys goes to zero. Finally, Figs. 5 and 6 show that for the thinnest YBCO layers the superlattice T_{c0} is quite sensitive to the number of adjacent YBCO cells in a layer.

Several different effects may contribute to the dependence of T_{c0} on the PBCO and YBCO layer thicknesses. Moreland et al. [36] have reported forming a superconducting Josephson point contact between two YBCO films coated with 5 nm of Ag, in the squeezable electron tunneling geometry. The Ag layer was believed to become superconducting by proximity effect coupling. Although ξ_c is expected to diverge as $(1-T/T_c)^{-1/2}$, the very small and T-dependent carrier concentration in the PBCO layers of our superlattices should make any proximity effect contribution largest for the thicker (higher T_{c0}) YBCO layers and for the thinnest PBCO layers. Rogers et al. [37] also recently observed weak dc and ac Josephson effects in YBCO/PBCO/YBCO trilayer structures in which the PBCO layers were 50 nm thick. Evidence for Josephson effects through such thick layers suggests that Josephson coupling may also affect the T_{c0} of our superlattices, and might even imply that inter-cell coupling is responsible for YBCO's high "intrinsic" thin-film $T_{c0} \geq 92$ K.

However, an alternative interpretation of our data is that a single-cell-thick YBCO layer has an intrinsically high T_{c0}, but that a YBCO cell's electronic structure is severely modified by being located adjacent to PBCO. From Fig. 6 it can be seen that most of the increase in T_{c0} with increasing YBCO layer thickness occurs as the first few YBCO cells are added, i.e., 3- or 4-cell-thick YBCO layers have much higher T_{c0} than single-cell-thick YBCO, but T_{c0} increases only slightly for still thicker YBCO layers. This T_{c0} behavior is consistent with the thicker YBCO layers not being affected much by PBCO, because they are composed mostly of "interior" YBCO cells.

Wood has recently shown[38] that a hole-filling mechanism, together with earlier results from a spin-polaron model of high-T_c superconductivity, provides excellent agreement with the experimental T_c data for both $Y_{1-y}Pr_yBa_2Cu_3O_{7-x}$ alloys and for our superlattices (Figs. 5 and 6). The ingredients of Wood's model are as follows. First, the spin-polaron model is used to give the behavior of T_c as a function of the hole concentration in a single CuO_2 plane, by solving a BCS-like equation for T_c under certain simplifying assumptions. The single hole in a unit cell of $YBa_2Cu_3O_7$ is found to be distributed approximately 0.6 on the chain plane and 0.2 on each of the two CuO_2 planes, in agreement with Hall effect measurements. [39] Removal of oxygen from the chain plane results in a nonlinear depletion of the hole concentration in both planes, and a resulting decrease in T_c. For $Y_{1-y}Pr_yBa_2Cu_3O_{1-x}$ alloys, Wood treats Pr as having a valence of +4, thus providing an additional electron relative to Y, i.e. Pr "dopes" YBCO with electrons. Consequently, addition of Pr to YBCO causes electrons to be distributed among the chain and CuO_2 planes, with the average number of holes per unit cell in $Y_{1-y}Pr_yBa_2Cu_3O_{7-x}$ being 1-y. Wood shows that this model reproduces the experimentally observed decrease in T_c with increasing Pr content, with T_c ~ 0 K for $0.5 < y < 0.6$. For our YBCO/PBCO superlattices, Wood assumes that similar electron doping occurs, with two important additional requirements: (1) The electrons from Pr redistribute themselves among the various types of of YBCO and PBCO cells so as to minimize the total energy, and (2) charge neutrality is maintained over the supercell composed of

M(Y) + N(Pr) cells (one superlattice period). Using this procedure, Wood has calculated the variation of T_c(midpoint) as a function of both the YBCO and PBCO layer thicknesses, and obtained results in excellent agreement with the data of Figs. 5 and 6.

As Wood points out, this agreement seems too good to be merely fortuitous, so it is interesting to examine both the details and the uniqueness of his model. With regard to the electron-doping process, Wood finds (within the limits of some numerical approximations and simplifications) that the largest electron transfer from PBCO occurs for the 1×1 superlattice structure, for which each YBCO cell acquires ~0.32 electrons. For the 1×2 structure, each YBCO cell acquires ~0.38 electrons, but since there are two PBCO cells per supercell, each PBCO cell gives up only ~0.19 electrons. For structures in which M or N ≥ 3, there can be two or more types of unit cells within the YBCO and/or PBCO layers, i.e., various types of "interior" cells and "boundary" cells. For example, for the 3(Y) × 16(Pr) structure with T_{c0} ~ 71 K (Fig. 6), Wood finds that the single interior YBCO cell acquires only ~0.23 electron while the two boundary YBCO cells receive ~0.31 electron each from the 16-cell-thick PBCO layer. Consequently, the interior YBCO cell goes superconducting at a higher temperature than the two outer cells. According to Wood, it is the fact that the YBCO cells added beyond N(Y) = 3 are well-isolated from the YBCO/PBCO interface that causes T_c to increase much less rapidly with increasing N(Y), resulting in the "knee" in T_{c0} vs. N(Y) in Fig. 6.

Regarding uniqueness, Wood points out that a spin-polaron superconductive pairing mechanism is not necessarily required, and that any other mechanism that leads to the correct dependence of T_c on the number of holes in a CuO_2 plane may work equally well. He also finds that although superconducting pair-breaking by Pr local moments might be incorporated in the calculations, it clearly is not needed to explain the T_c data. Similarly, no coupling was assumed between the two CuO_2 planes in a unit cell, or between the pairs of planes in adjacent cells, so although such coupling cannot be ruled out (again, provided it produces the required T_c vs. hole concentration behavior), it does not seem to be needed.

From these considerations it is clear that it will be of great interest to carry out additional superlattice experiments in which the composition of the insulating layers is significantly changed, both in order to test the electron-doping idea more definitively, and to determine whether there are less-perturbing boundary conditions for which the T_{c0} of single-cell-thick YBCO layers can be much higher than the ~19 K value found here. Such experiments also could help to determine whether other mechanisms also are active, e.g., Josephson coupling between layers. In connection with such experiments we note that Kanai et al.[40] recently fabricated $Bi_2Sr_2(Ca_{1-x}Y_x)_1Cu_2O_8$-based superlattices in which two different Y concentrations, x = 0.15 and x = 0.5, are alternated to produce superconducting and semiconducting layers, respectively. Using semiconducting to superconducting layer thicknesses in the ratios of 8/4, 4/2, and 2/1 Kanai et al. found that the superlattice transition temperatures were unaffected by the superlattice periodicity, in striking contrast to our results for YBCO/PBCO superlattices. They attribute the apparent independence of the superconducting layers' T_c from their environment or coupling with other superconducting layers to the highly two-dimensional character of $Bi_2Sr_2(Ca_{1-x}Y_x)_1Cu_2O_8$.[40]

4.2 Critical Current Density

The lack of any enhancement of $J_c(H = 0)$ in our initial measurements on YBCO/PBCO superlattices contrasts with recent results of Gross et al. for $Nd_{1.83}Ce_{0.17}CuO_x/YBa_2Cu_3O_{7-y}$ (NCCO/YBCO) superlattices.[41] Their structures were prepared under oxidizing conditions so that only the YBCO layers are superconducting, with the NCCO layers acting as nonsuperconducting spacers. Gross et al. found an approximately order-of-magnitude increase in $J_c(H = 0)$, from J_c ~ 1 MA/cm^2 for a 20 nm thick YBCO film to J_c ~ 10–11 MA/cm^2 for a 40 nm(Nd)/20 nm(Y) superlattice, with J_c decreasing for larger Nd-layer thicknesses. They attributed this peak in the J_c-enhancement to formation of interfacial misfit dislocations, whose density is know to reach a maximum for layer thicknesses just above the critical thickness for strain field relaxation.[42] The dislocations presumably act as additional flux-pinning centers. The NCCO/YBCO and PBCO/YBCO multilayer systems are similar in that the insulating layers are in compression in the a-b plane and the superconducting YBCO layers are in tension. However, for the NCCO/YBCO system the biaxial tension removes the orthorhombic distortion and makes the YBCO unit cell isotropic (a = b) in the basal plane. In PBCO, the a (b) lattice constant is only ~ 1.0% (1.2%) larger than in YBCO, so the absence of any J_c enhancement in the YBCO/PBCO superlattices that we have measured to date could indicate either that they are coherently strained at these layer thicknesses or, if dislocations have formed, that their density is low enough that the additional flux-pinning is small.

5. SUMMARY AND CONCLUSIONS

We have shown that the pulsed-laser deposition method can be employed to grow epitaxial, nonsymmetric M(Y) x N(Pr) superlattices in which $YBa_2Cu_3O_{7-x}$ (YBCO) layers either M = 1, 2, 3, 4, 8, or 16 c-axis unit cells thick are separated by insulating $PrBa_2Cu_3O_{7-x}$ (PBCO) layers N unit cells thick (N = 1 to ~32). We find that the zero-resistance superconducting transition temperature, T_{c0}, initially decreases rapidly with increasing PBCO layer thickness, but then saturates at T_{c0} ~ 19 K, 54 K, 71 K, or 80 K, for structures containing 1-, 2-, 3-, or 4-cell-thick YBCO layers, respectively. Critical current density measurements carried out on structures containing somewhat thicker (16- or 32-cell thick) YBCO layers show that both the magnitude of $J_c(H = 0)$ ~ 1-2 MA/cm^2, as well as the magnetic field-dependence and the anisotropy of $J_c(H)$, all are in good agreement with corresponding measurements for thicker, single-layer YBCO films. In particular, there is no evidence of an enhanced $J_c(H)$ due to the multi-layered structure, for the layer thicknesses investigated to date. Other experiments suggest that the systematic variation of T_{c0} that we observe, as a function of the YBCO and PBCO layer thicknesses, may include effects due to Josephson coupling between the YBCO layers (through relatively thick PBCO layers), but an alternative explanation, in terms of "electron doping" of the YBCO layers that are nearest to the PBCO layers, also has been suggested and fits our results very well. Further experiments, in which the composition of the insulating layers is significantly changed, will be very useful to distinguish between these mechanisms and to further test the electron-doping idea.

6. ACKNOWLEDGMENTS

We would like to thank R.F. Wood for several discussions and for permission to refer to his work prior to publication, P. H. Fleming for assistance with sample characterization, and B. C. Sales for the PBCO target preparation. This research was sponsored by the Division of Materials Sciences, U. S. Department of Energy under contract DE-AC05-84OR21400 with Martin Marietta Energy Systems, Inc.

7. REFERENCES

1. K. Hirata, K. Yamamoto, K. Iijima, J. Takada, T. Terashima, Y. Bando, and H. Mazaki, *Appl. Phys. Lett.* 56, 683 (1990).
2. J. J. Kingston, F. C. Wellstood, P. Lerch, A. H. Miklich, and J. Clarke, *Appl. Phys. Lett.* 56, 189 (1990).
3. T. Kimura, H. Yamawaki, Y. Arimoto, K. Ikeda, M. Ihara, and M. Ozeki, *Mat. Res. Soc. Symp. Proc.* 53, 143 (1986).
4. X. D. Wu, A. Inam, M. S. Hegde, B. Wilkens, C. C. Chang, D. M. Hwang, L. Nazar, and T. Venkatesan, *Appl. Phys. Lett.* 54, 754 (1989).
5. J. M. Phillips, *Mat. Res. Soc. Symp. Proc.* 37, 143 (1985).
6. H. Fukumoto, T. Imura, and Y. Osaka, *Jap. J. Appl. Phys.* 27, L1404 (1988).
7. D. K. Fork, D. B. Fenner, G. A. N. Connell, J. M. Phillips, and T. H. Geballe, submitted to *Applied Physics Letters*.
8. M. Ishida, I. Katakabe, T. Nakamura, and N. Ohtake, *Appl. Phys. Lett.* 52, 1326 (1988).
9. D. K. Fork, D. B. Fenner, and T. H. Geballe, submitted to *Applied Physics Letters*.
10. G. W. Morris, R. E. Somekh, Z. H. Barber, E. J. Williams, W. W. Schmahl, and J. E. Evetts, Materials Research Society Symposium Proceedings 169 (in press).
11. A. B. Berezin, C. W. Yuan, and A. L. de Lozanne, *Appl. Phys. Lett.* 57, 90 (1990).

12. F. Konushi, T. Doi, H. Matsunaga, Y. Kakihara, M. Koba, K. Awane, and I. Nakamura, *Mat. Res. Soc. Symp. Proc.* 56, 259 (1986).
13. K. Char, N. Newman, S. M. Garrison, R. W. Barton, R. C. Taber, S. S. Laderman, and R. D. Jacowitz, *Appl. Phys. Lett.* 57, 409 (1990).
14. D. H. Lowndes, D. P. Norton, and J. D. Budai, *Phys. Rev. Lett.* 65, 1160 (1990).
15. D. H. Lowndes, D. P. Norton, J. D. Budai, S. J. Pennycook, D. K. Christen, B. C. Sales, and R. Feenstra, Materials Research Society Symposium Proceedings **191** (in press).
16. B. Okai, M. Kosuge, H. Nozaki, K. Takahashi, and M. Ohta, *Jap. J. Appl. Phys.* 27, L41 (1988).
17. J. L. Peng, P. Klavins, R. N. Shelton, H. D. Radousky, P. A. Hahn, and L. Bernardez, *Phys. Rev. B* 40, 4517 (1989).
18. D. P. Norton, D. H. Lowndes, R. Feenstra, and J. D. Budai, to be published.
19. J.-M. Triscone, M. G. Karkut, L. Antognazza, and O. Fischer, *Phys. Rev. Lett.* 63, 1016 (1989).
20. J.-M. Triscone, O. Fischer, O. Brunner, L. Antognazza, A. D. Kent, and M. G. Karkut, *Phys. Rev. Lett.* 64, 804 (1990).
21. Q. Li, X. X. Xi, X. D. Wu, A. Inam, S. Vadlamannati, W. L. McLean, T. Venkatesan, R. Ramesh, D. M. Hwang, J. A. Martinez, and L. Nazar, *Phys. Rev. Lett.* 64, 3086 (1990).
22. C. T. Rogers, A. Inam, M. S. Hegde, B. Dutta, X. D. Wu, and T. Venkatesan, *Appl. Phys. Lett.* 55, 2032 (1989).
23. T. Venkatesan, A. Inam, B. Dutta, R. Ramesh, M. S. Hegde, X. D. Wu, L. Nazar, C. C. Chang, J. B. Barner, D. M. Hwang, and C. T. Rogers, *Appl. Phys. Lett.* 56, 391 (1990).
24. X. D. Wu, X. X. Li, Q. Li, A. Inam, B. Dutta, L. DiDomenico, C. Weiss, J. A. Martinez, B. J. Wilkens, S. A. Schwartz, J. B. Barner, C. C. Chang, L. Nazar, and T. Venkatesan, *Appl. Phys. Lett.* 56, 400 (1990).
25. C. T. Rogers, A. Inam, J. B. Barner, R. Ramesh, and T. Venkatesan, Proc. Int. Cryogenic Materials Conf. (May, 1990, Garmisch, Fed. Rep. Germany).
26. D. H. Lowndes, D. P. Norton, J. W. McCamy, R. Feenstra, J. D. Budai, D. K. Christen, E. Jones, and D. Poker, in *High Temperature Superconductors: Fundamental Properties and Novel Materials* (ed. by D. Christen, P. Chu, J. Narayan, and L. Schneemeyer, Materials Research Society, Pittsburgh, PA) in press.
27. A. Inam, C. T. Rogers, R. Ramesh, L. Farrow, K. Remschnig, D. Hart, and T. Venkatesan, *Applied Physics Letters* (in press).
28. J. D. Budai, R. Feenstra, and L. A. Boatner, *Phys. Rev. B* 39, 12355 (1989).
29. I. K. Schuller, *Phys. Rev. Lett.* 44, 1597 (1980).
30. S. J. Pennycook and D. E. Jesson, *Phys. Rev. Lett.* 64, 938 (1990).
31. S. J. Pennycook, M. F. Chisholm, D. E. Jesson, D. P. Norton, J. W. McCamy, and D. H. Lowndes, *Materials Research Society Symposium Proceedings* 169 (in press).
32. D. B. McWhan, in *Synthetic Modulated Structures* (ed. by L. L. Chang and B. C. Giessen, Academic Press, Orlando, FL, 1985), p. 60.
33. D. K. Christen, C. E. Klabunde, J. R. Thompson, H. R. Kerchner, S. T. Sekula, R, Feenstra, and J. D. Budai, *Physica C* 162-164, 653 (1989).
34. D. K. Christen, C. E. Klabunde, R. Feenstra, D. H. Lowndes, D. P. Norton, J. D. Budai, H. R. Kerchner, J. R. Thompson, L. A. Boatner, J. Narayan, and R. Singh, *Physica B* 165-166, 1415 (1990).
35. B. Roas, L. Schultz, G. Saemann-Ischenko, *Phys. Rev. Lett.* 64, 479 (1990).
36. J. Moreland, R. H. Ono, J. A. Beall, M. Madden, and A. J. Nelson, *Appl. Phys. Lett.* 54, 1477 (1989).
37. C. T. Rogers, A. Inam, M. S. Hegde, B. Dutta, X. D. Wu, and T. Venkatesan, *Appl. Phys. Lett.* 55, 2032 (1989).
38. R. F. Wood, submitted to *Physical Review Letters*.
39. Z. Z. Wang et al., *Phys. Rev. B* 36, 7222 (1987).
40. M. Kanai, T. Kawai, and S. Kawai, *Appl. Phys. Lett.* 57, 198 (1990).
41. R. Gross, A. Gupta, E. Olsson, A. Segmuller, and G. Koren, *Appl. Phys. Lett.* 57, 203 (1990).
42. D. Ariosa, O. Fischer, M. G. Karkut, and J.-M. Triscone, *Phys. Rev. B* 37, 3421 (1988).

- END -

DATE FILMED

11 / 1 / 90